Computational approach to identify structural and elastic relationship in metastable crystalline and amorphous alloy thin films: Mo1-xNix and Mo1-xSix case studies

Chen Hui Li, Cristiano Poltronieri, Grégory Abadias, Philippe Djemia

Computational approach to identify structural and elastic relationship in metastable crystalline and amorphous alloy thin films: $Mo_{1-x}Ni_x$ and $Mo_{1-x}Si_x$ case studies

Chen Hui Li[1], C. Poltronieri[2], G. Abadias[3], P. Djemia[2]

[1]State Key Laboratory of Superlattices and Microstructures, Institute of Semiconductors, Chinese Academy of Sciences, Beijing 100083, China

[2]LSPM- CNRS 3401, Université Paris 13, 99 Avenue J.B. Clément, 93430 Villetaneuse, France

[3]Institut Pprime, UPR 3346 CNRS, Université de Poitiers, 86073 Poitiers, France

Abstract

Previously well-established experimental trends of ground-state properties of crystalline and amorphous $Mo_{1-x}Si_x$ and $Mo_{1-x}Ni_x$ alloys with $0 \leq x \leq 1$ are predicted by first-principles calculations and inter-relationship with sound velocities and elastic properties are identified. The free energy of mixing, calculated at 300K provides accurate values of the critical Si and Ni concentrations leading to the crystalline-to-amorphous transition. Specifically, a transition from BCC to amorphous state is predicted for $x_{Si} \sim 0.14$ and $x_{Ni} \sim 0.32$, while FCC to amorphous transition is observed for $x_{Ni} \sim 0.77$. These structural transitions are accompanied by modifications of the out-of-plane longitudinal modulus C_{33}, and out-of-plane shear modulus C_{44}. In the crystalline region, a pronounced softening of C_{44} and C_{33} is predicted for both solid solution alloys. While for amorphous Mo-Ni, the elastic constants do not undergo significant changes, for amorphous Mo-Si, they exhibit two distinct behaviors depending on the electronic properties and bonding character. For $0.2 \leq x_{Si} \leq 0.7$, the metallic character of the amorphous alloys is maintained and the elastic properties are remarkably stable. For $x_{Si} > 0.7$, a progressive increase in the atomic volume is observed and the amorphous alloys acquire a covalent character and a reduced coordination number. Surprisingly, during this transition, both the longitudinal and shear acoustic velocities continuously increase, despite a

progressive softening of the elastic stiffness constants. These calculations provide deep insight at the atomic-scale and reproduce satisfactorily the earlier experimental works of magnetron co-sputtered Mo-Si films, while some disagreement on elastic properties remain for more energetic ion beam sputtered Mo-Ni films, likely partially attributed to point-defects.

Keywords : *ab initio* molecular dynamics ; density functional theory ; special quasi-random structures; elastic constants ; metallic glass

1. Introduction

In nanoscale multilayered structures, the physical properties and more specifically the elastic behavior have been shown to exhibit deviations compared to the bulk properties of the constitutive materials [1]. Elastic anomalies have been observed in superlattices with small modulation wavelengths (a few nm) highlighting the role of interfaces versus bulk properties. Surprisingly, such effects have been also reported in systems made of immiscible elements [2-5]. From a phenomenological point of view, the observed softening can be ascribed to an interfacial zone exhibiting anomalous elastic properties. Stress/strain, topological and chemical disorder, enhanced solubility or amorphization are possible sources of such interfacial softening. Experimentally, Brillouin light scattering (BLS) [4, 5] and picosecond ultrasonics (PU) [6, 7] techniques have proven to be complementary in measuring the elastic properties of various metallic multilayers. The softening of some effective elastic constants has been reported in various systems, such as in Cu/W [2], Mo/Ni [3-5] and Pt/Ni or Ti/Ni [3]. In the metal/oxide $Ni_{80}Fe_{20}/Al_20_3$ multilayers [7], with no intermixing at the interface, Rossignol *et al.* also found an anomalous behavior of C_{33} and C_{44} elastic constants, measured by PU and BLS, respectively, as function of the bilayer period, which could also be ascribed to a weak interfacial bonding but not to a modified structure at the interface.

By contrast, there also exist systems with a modified interface layer, for which no anomalous behavior of elastic constants has been observed, such as for Mo/Si multilayers studied by PU [6]. In that case, high-resolution transmission electron microscopy observations of the samples confirmed the strong asymmetry of the interfaces with the existence of an amorphous silicide interfacial layer at the Mo-on-Si interface, identified as $MoSi_2$ and extending over up to ~2 nm [8, 9], whereas the Si-on-Mo interface is mainly characterized by a rough profile.

In binary alloys, phase transitions are also accompanied by strong variations of the elastic properties. This is the case of $Mo_{1-x}Ni_x$ thin films produced by ion-beam sputtering [4, 5], for

which the variations of C_{44} and C_{33} elastic constants have been reported from PU and BLS measurements [10]. X-ray diffraction (XRD) results, also presented in these works, evidence the formation of solid solutions at both ends of the phase diagram and an extended amorphous region is observed for $0.27 < x_{Ni} < 0.73$. This range matches well the one ($0.3 < x_{Ni} < 0.6$) observed by Zhao *et al.* [11], which is a little wider than that obtained from their calculated free-energy diagram ($0.48 < x_{Ni} < 0.62$). Glass-forming range of MoNi was derived from molecular dynamics simulations by Zhang *et al*. [12] with a satisfactory agreement $0.25 < x_{Ni} < 0.79$. The alloying of Mo and Ni is found to decrease the intrinsic stacking fault energy of the solid solution from 150 mJ/m^2 (pure Ni) to 50 mJ/m^2 (82.5 at.% Ni) almost linearly [13]. The first-principles calculations of composition-dependent thermal expansion, thermal electronic excitation and the magnetic transition are shown to be the main factors rendering the complex variations in the elastic properties and twinning behavior of Ni-Mo solid solution with temperature [14], with Mo addition increasing the solid solution ductility. A detailed and extensive literature review of the Mo–Ni binary system thermodynamic modeling can be find in Ref. [15], with a discussion of the existence of several stable intermetallics such as $MoNi_2$ and $MoNi_8$.

A complementary study of elastic properties on sputter-deposited $Mo_{1-x}Si_x$ films was also performed, combining PU and BLS [16], with XRD results, showing formation of solid solutions and an amorphous region extending above x_{Si}~0.19. In this system, there exist three intermediate ordered phases [17], Mo_3Si, Mo_5Si_3, and $MoSi_2$, but not observed in amorphous compositional range of these films. For both systems, Mo-Ni and Mo-Si, prior experimental works [4, 6, 10, 16] have therefore provided accurate data covering the whole compositional range, among them: phase analysis retrieved from XRD, mass density and atomic volume measured by X-ray reflectivity (XRR), sound velocities and elastic constants obtained by PU and BLS. However, the atomistic-scale understanding of these established trends, in particular

the link between structural and mechanical evolutions on either side of the crystalline-to-amorphous transition, remains to be investigated theoretically.

In the present study, we investigate by first-principles calculations the structural (interatomic distance d_{av}, atomic volume V_{at} and mass density ρ) and elastic properties (shear and longitudinal elastic moduli, C_{44} and C_{33}, respectively) of $Mo_{1-x}Ni_x$ and $Mo_{1-x}Si_x$ alloys in the entire chemical composition range, covering both BCC or FCC crystalline and amorphous phases. *Ab initio* molecular dynamics (AIMD) and special quasi-random structures (SQS) method are used to design the amorphous alloys, and BCC or FCC crystalline random solid solutions, respectively. All numerical results are compared to the existing experimental data [4, 6, 10, 16] and discussed in relation with topological analysis of the amorphous state to provide insights on local atomic configurations region and its role. In addition, metal-to-insulator transition in the Mo-Si system is also discussed based on density of electronic states calculations. Overall, the computed data show a good agreement with experimental trends, shedding light on the inter-relationships between atomic scale structural and physical properties.

2. Numerical methods

2.1 Special quasi-random structures (SQS) for the crystalline cubic phases

First-principles calculations based on density functional theory (DFT) were performed utilizing the Vienna *Ab initio* Simulation Package (VASP) [18]. Special quasi-random supercells [19] with 54 and 108 atoms, were built as input atomic structures, to mimic the random crystalline BCC- and FCC-alloys in Mo-Si and Mo-Ni systems. The calculations were done with the standard projector augmented wave (PAW) pseudopotentials provided by the code. The exchange and correlation interaction between electrons were described by the Perdew-Burke-Ernzerhof (PBE) functional [20]. The cutoff energy of 350 eV for the plane-

wave-basis set was fixed for all the calculations to ensure well-converged results. For Ni-rich compositions, spin-collinear option was employed to take into account the ferromagnetic properties. The conjugate gradient algorithm was utilized for geometry optimization. The optimization stopped when the norms of all the forces are smaller than 0.01 eV/Å.

The three independent single crystal elastic constants c_{11}, c_{12} and c_{44} were computed at 0 K using the stress-strain method ($\sigma = c\varepsilon$) [21], considering both relaxed and unrelaxed atomic positions after each applied strain. We used here the quasi-Newton algorithm to relax atoms, in this case, the stopping force criterion was 0.05 eV/Å. Effective elastic constants were also computed for direct comparison with experiments. For polycrystalline materials with a preferential crystal orientation (in the present case <110>-textured Mo-rich BCC alloys (Mo-Ni and Mo-Si systems) and <111>-textured Ni-rich FCC alloys), the elastic symmetry is hexagonal, such that five independent elastic constants C_{11}, C_{12}, C_{33}, C_{13}, C_{44}, are needed. These effective C*ij* were calculated by Voigt-Reuss-Hill averages [22] considering the experimentally observed preferred crystal orientations [4, 5, 16]. Then longitudinal and shear wave velocities could be determined using the relation $C_{33} = \rho v_L^2$ and $C_{44} = \rho v_S^2$, with C_{33} and C_{44} corresponding to the out-of-plane longitudinal and shear effective modulus. These are the relevant parameters to calculate for comparison to experimental data measured by PU (C_{33}, v_L) and BLS (C_{44}, v_s). In the simpler case of amorphous materials (isotropic case), $C_{33} = C_{11}$. To validate most of the used parameters, we checked the good agreement between our elastic constant calculated for Mo and Ni with their bulk ones (Mo: C_{33} = 459 GPa, C_{44} = 111 GPa; Ni: C_{33} = 347 GPa, C_{44} = 66 GPa). Similarly, we compared our elastic constant calculated for a-Si with previous calculations (C_{11} = 139 GPa, C_{44} = 34 GPa) [23] and experiments (C_{11} = 156 GPa, C_{44} = 48.8 GPa) [24].

2.2 *Ab initio* molecular dynamics (AIMD) and cluster analysis for the amorphous phase

Amorphous alloys were designed by AIMD calculations, to examine the local atomic arrangement in relation to chemical composition and its impact on structural and mechanical properties in both Mo-Ni and Mo-Si systems. A cubic box with periodic boundary conditions was used, containing 256 atoms of the desired alloy composition. Initially, all alloys were heated to 3500 K and equilibrated for a minimum of 10 picoseconds (ps) under isobaric-isothermal (NPT) ensemble, providing homogeneous molten alloys with relaxed atomic positions. Amorphous solid state was obtained from cooling down the equilibrated melt from 3500 K to 300 K at a cooling rate of 1.06×10^{15} K/s (time step of 1.5 fs and 2000 steps, total cooling time of 3 ps), using the isovolumic-isothermal (NVT) ensemble and the Nose thermostat, followed by a relaxation of the cell with NPT ensemble and Langevin thermostat for at least 15 ps by steps of 1.5 fs (more than 10 000 steps). The atomic volume and mass density, together with pair distribution function of atoms (PDF), were subsequently determined. Our criterion of successful production of the amorphous supercell, was the limited variation of averaged atomic volume (less than 0.1 $Å^3$/at.) that we can satisfactorily compare to experiments (even more stringent for MoSi case) and of averaged total energy (less than a few meV/at.), during last NPT relaxation runs. To check the influence of the cooling time τ_c on the resulting amorphous structures, different AIMD simulations were run for $Mo_{40}Si_{60}$ alloy, varying the cooling time τ_c from 0.3 to 3 ps with a common 0.3 fs step, and comparing the final total energy and atomic volume obtained after the NPT runs. It was noticed by Houska *et al.* [25] for ZrSiN case (a transition metal alloyed with light elements) that the duration of the cooling should not be much lower than 2 ps for producing structures independent of the cooling rate. Our results showed only a moderate influence of τ_c, with a lower total energy ~-19 meV and lower volume ~-1% for the 0.3 ps cooling time, relative to the chosen parameter (τ_c =3 ps).

Similarly, the elastic constants c_{ij} of a given structure were investigated at 0 K using the stress-strain method ($\sigma = c\varepsilon$) [21], considering both relaxed and unrelaxed atomic positions after each applied strain. The same geometry optimization algorithms and force convergence criteria were used as for the crystalline phases.

The Voronoi tessellation method, implemented through the OVITO software package [26], was employed to analyze the last thousand-time steps of the quenched alloys. In this analysis, each polyhedral cell was assigned five indices < n3 n4 n5 n6 n7 >, where n_i (i≥ 3) represents the number of faces with i-edges in each Voronoi cell. Of particular interest were icosahedral structures denoted by the Voronoi index <0 0 12 0 0>, with the cluster-central atom coordination number (Σni) [27].

3. Results and discussion

3.1 Energetics and phase stability

The phase stability of the crystalline and amorphous alloys were firstly evaluated from DFT total energy calculations at 0 K for both systems. Based on the obtained formation enthalpies, the following compositional range for stable amorphous Mo-Ni ($0.45 < x_{Ni} < 0.95$) and Mo-Si ($x_{Si} > 0.32$) alloys was determined. These boundary regions do not perfectly match the reported experimental values ($0.27 < x_{Ni} < 0.73$ and $x_{Si} > 0.20$, for MoNi and MoSi systems, respectively). Additionally, we employed a simple analytical thermodynamic model with a finite temperature, in which the limits of the glass-forming compositional range (which is linked to the glass forming ability) of the alloys were defined by the compositions at which the free energy of formation of amorphous phase (ΔG_{am}) is lower than that of the crystalline counterpart (ΔG_{ss}) [28]. The free energy of mixing of a solid solution was calculated as

$$\Delta G_{ss} = \Delta H_{ss} - T\Delta S_{ss} \quad (1)$$

while, the amorphous one is defined as

$$\Delta G_{am} = \Delta H_{am} - T\Delta S_{am} \quad (2)$$

where ΔH_{ss}, ΔH_{am} and ΔS_{ss}, ΔS_{am} are the enthalpies and entropies of mixing of the crystalline and amorphous phase, respectively, and T is the absolute temperature. The enthalpies of mixing, or formation enthalpies, of amorphous and solid solution phases were evaluated following the model proposed by Van der Kolk *et al.* [29] with pure crystalline solid elements as a common reference.

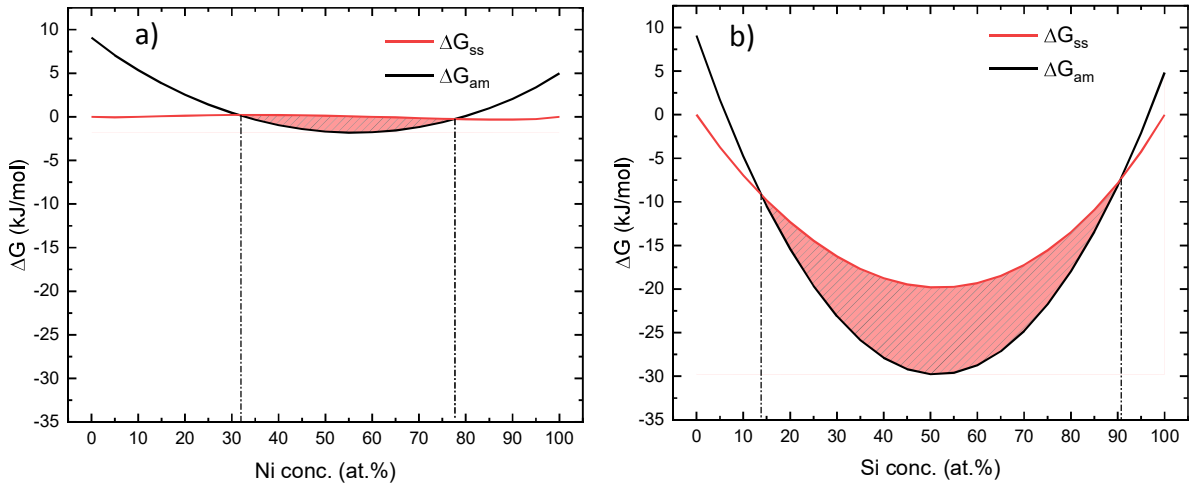

Figure 1: Free energy of formation of amorphous and crystalline phases calculated at 300 K with the Van der Kolk analytical model [29] for a) $Mo_{1-x}Ni_x$, and b) $Mo_{1-x}Si_x$. The dashed lines represent the predicted compositional amorphization range.

Figure 1 represents the free energies of mixing of the amorphous and crystalline phases calculated at 300 K. The compositional amorphization ranges for the two systems are highlighted by the dashed lines and they are identified where $\Delta G_{ss} - \Delta G_{am} > 0$. This approach has been used in other studies showing a good agreement between predicted and experimental glass-forming compositional range values for ZrNi, ZrCo and ZrCu alloys [28]. For Mo-Si alloy, the Van der Kolk model predicts a glass-forming compositional range

between 14 and 90 at. % Si (see Fig. 1b), while for Mo-Ni this compositional interval appears smaller and between 32 and 77 at. % Ni (see Fig. 1a). These predicted values are in closer agreement with the experimental results comparatively to DFT predictions [4, 16].

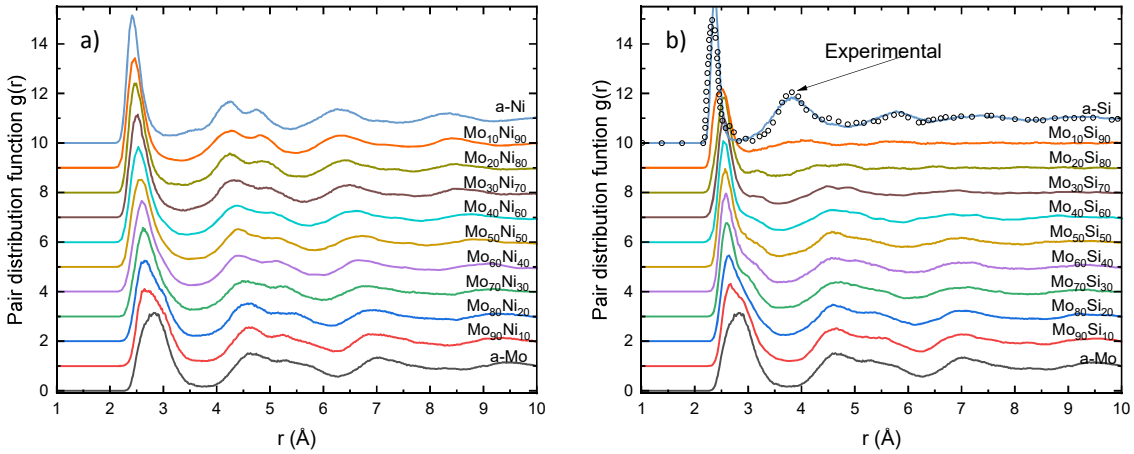

Figure 2: Calculated pair distribution function for a) $Mo_{1-x}Ni_x$, and b) $Mo_{1-x}Si_x$ amorphous alloys. One comparison is shown for pure Si with available experimental neutron-diffraction data on evaporated amorphous Si (a-Si) from Ref. [30].

3.2 Pair distribution function, interatomic distance and cluster analysis

Calculated pair distribution functions (PDF) of MoNi and MoSi amorphous alloys are depicted in Figure 2. Unfortunately, no experimental data are available for these systems except for evaporated amorphous silicon [30] that shows a good agreement with our calculation. The first peak located around 3 Å is related to the first-shell atomic coordination and its position to the average interatomic distance (d_{av}). Addition of Ni to Mo, leads to a continuous decrease of the average interatomic distance d_{av} (**see "interatomic distance" in supplementary materials**), as expected by Zen's mixing law [31] and the sequence of atomic radii (r_{Mo} (1.415 Å) >r_{Ni} (1.21 Å) > r_{Si} (1.185 Å)). Hence, average bond lengths are supposed

to shorten, too. Nevertheless, partial pair distances (PPD) of Mo-Mo, Mo-Ni and Ni-Ni in amorphous Mo-Ni alloys remain constant close to 2.8, 2.6 and 2.47 Å, respectively. In case of Si addition, the decrease of d_{av} is less pronounced in the compositional range $0.2 < x_{Si} < 0.8$, thereafter it drops quickly. By contrast to Mo-Ni, PPD of Mo-Mo in amorphous Mo-Si alloys increases continuously from 2.85 to 3.25 Å, while PPD of Mo-Si alloys stay constant ~2.6 Å and the one of Si-Si first increases from 2.52 to 2.62 Å for x_{Si}~0.4 and then decreases for $x_{Si} > 0.7$ to ~2.4 Å for amorphous Si (a-Si).

Voronoi tessellation analysis was carried out to better investigate the short-range order (SRO) related to the atomic packing. Higher glass forming ability (GFA) has been observed in several metallic glasses [32-35] containing a maximum population fraction of full-icosahedra < 0 0 12 0 0 >. In particular, Abbasi *et al*., [36] proved that in ZrCuAl metallic glasses, low-volume Al- and Cu-centered clusters are responsible for the GFA, increasing the mass density and stabilizing the amorphous structure. Hence in this study, Ni- and Si-centered clusters are expected to be responsible for the increase in GFA of these alloys because of their lower volume. As shown in Figure 3, Si-centered clusters volume is decreasing from ~15 to 11 $Å^3$ above x_{Si}~0.2 while Ni-centered clusters volume remains roughly constant ~11 $Å^3$. Higher volumes are found for Mo-centered clusters, 18-16 $Å^3$ and 15.5-16 $Å^3$, for Mo-Si and Mo-Ni amorphous alloys, respectively.

Figure 4 shows the predominance of clusters with a coordination number of 12-15 for both systems (with the exception of Si-rich alloys, as it will be discussed hereafter). This common peculiar atomic coordination of 12-15 for metallic glasses (see Figure 4) was also related to the maximum shear resistance behavior [37, 38] and thermal stability [39] of metallic glasses. Additionally, Guo [40] suggested to consider also other slightly distorted icosahedra (*quasi*-icosahedra) identified by the indices < 0 2 8 1 0 >, < 0 2 8 2 0 >, < 0 1 10 2 0 > which are the most similar full-icosahedra among all polyhedra.

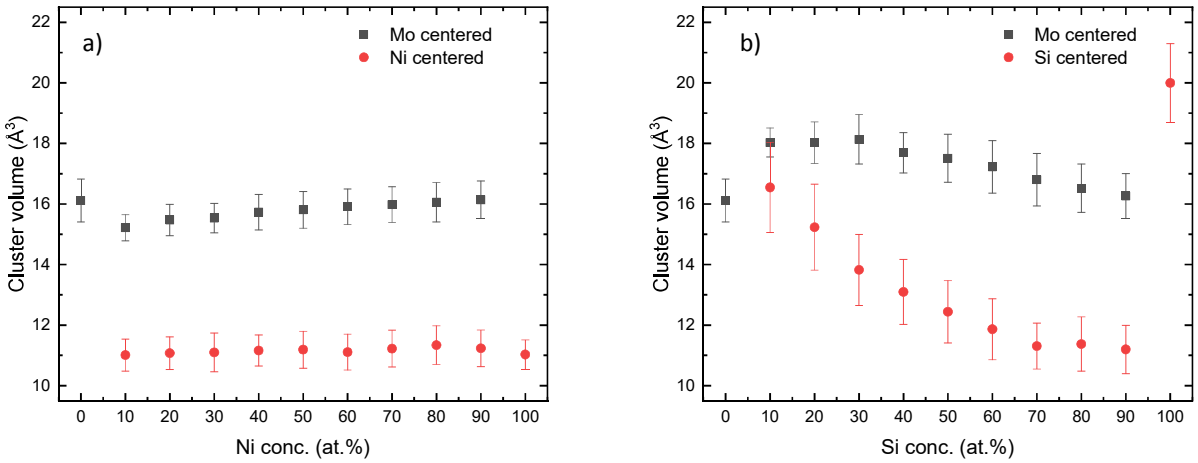

Figure 3: Mo-, Ni- and Si-centered clusters volume analysis for amorphous a) $Mo_{1-x}Ni_x$, and b) $Mo_{1-x}Si_x$ alloys.

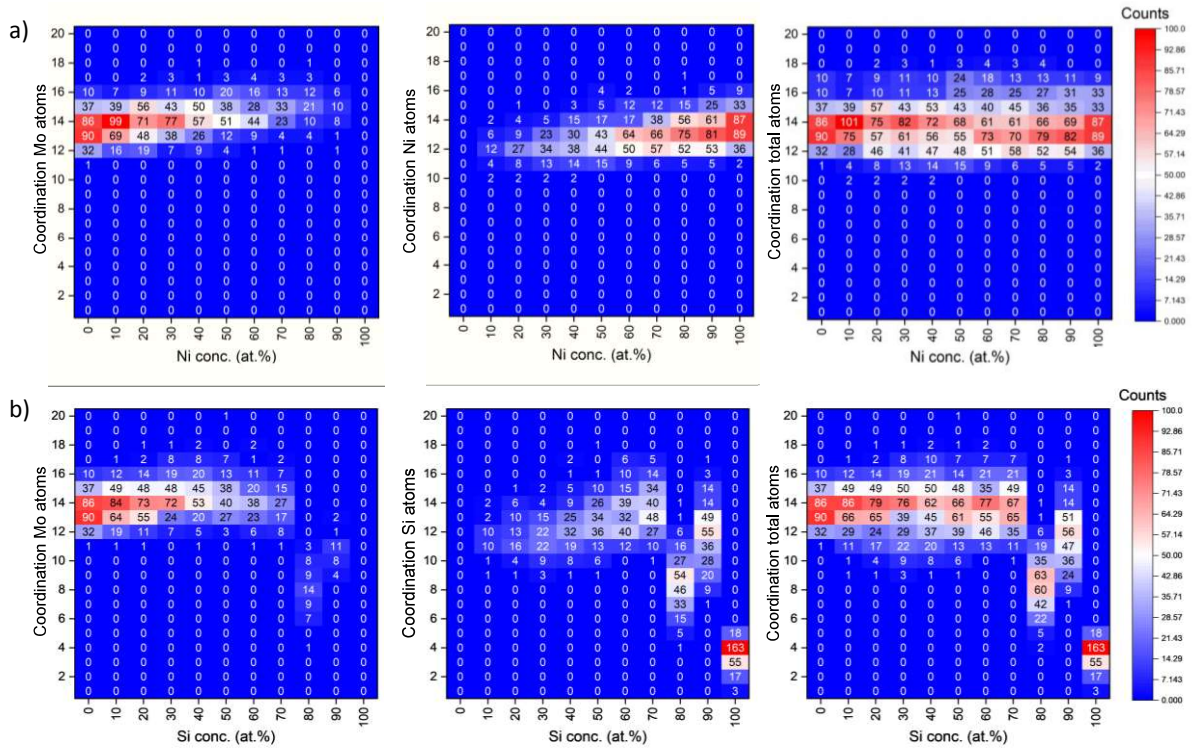

Figure 4: Mo-, Ni- and Si-centered clusters coordination analysis for amorphous a) $Mo_{1-x}Ni_x$, and b) $Mo_{1-x}Si_x$ alloys.

Figure 5 shows the polyhedral population of full- and *quasi*-icosahedra found in Mo-Ni and Mo-Si alloys. In the amorphous compositional range of Mo-Ni, the population fraction of

both Mo- and Ni-centered clusters shows a constant value around 5% and 25%, respectively. The maximum in Ni-centered cluster, associated to the maximum in GFA, was found between 10 and 70 at. % Ni which is consistent with the experimental compositional range of amorphization [4, 10]. However, Mo-Si alloys show a monotonic decrease in the population fraction of both Si- and Mo-centered clusters from 40 and 15%, respectively, to ~0% when the Si content is higher than 70 at. %. The absence of full- and quasi-icosahedra for Si content higher than 70 at.% is linked to a change in atomic-packing configuration and a reduction of atomic coordination, from 12-15 for metallic glasses to 4 for covalent a-Si (see Figure 4). This variation is correlated to a transition visible on atomic volume (discussed in next Section, see Figure 5) and elastic response (see section 3.5, further softening of C_{33} and C_{44}). Indeed, the volume of Si-centered clusters is much more affected, decreasing from 15 Å^3 for x_{Si}~0.20 to 11 Å^3 for $0.90 \geq x_{Si} \geq 0.70$ and increasing abruptly to 20 Å^3 for a-Si (see Figure 3). At the same time, the volume of Mo-centered clusters slightly decreases from 17.5 to 15.5 Å^3.

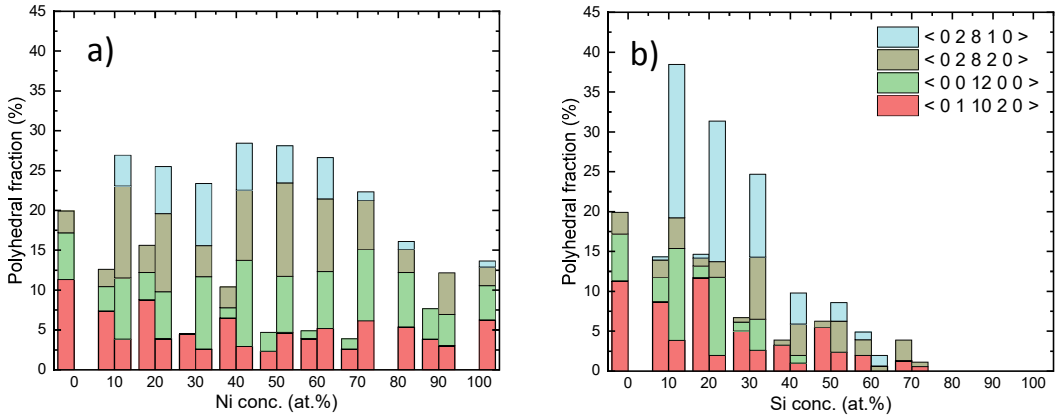

Figure 5: Voronoi full- and *quasi*-icosahedral population of a) $Mo_{1-x}Ni_x$ and b) $Mo_{1-x}Si_x$ amorphous alloys. For each composition, Mo-centered analyzed clusters are on the left while Ni- or Si-centered ones are on the right.

3.3 Atomic volume and mass density

The measured [4, 6, 10, 16] and calculated mass density (ρ) and atomic volume (V_{at}) of Mo-Ni and Mo-Si alloys are shown in Figure 6 as black circles. It can be observed that the numerical simulations consistently and quantitatively reproduce the experimental data. The mass density is found to continuously decrease from ~10.2 to ~8.9 g/cm^3 and to ~2.1 g/cm^3, for both Mo-Ni and Mo-Si alloys when Ni or Si is added to Mo, respectively. While the atomic volume of Mo-Ni is decreasing monotonously from ~15.5 to ~11 Å^3, the one of Mo-Si is first decreasing until x_{Si} ~ 0.5 before increasing rapidly beyond x_{Si} ~0.70 and reaching the highest value of ~20 Å^3 for a-Si.

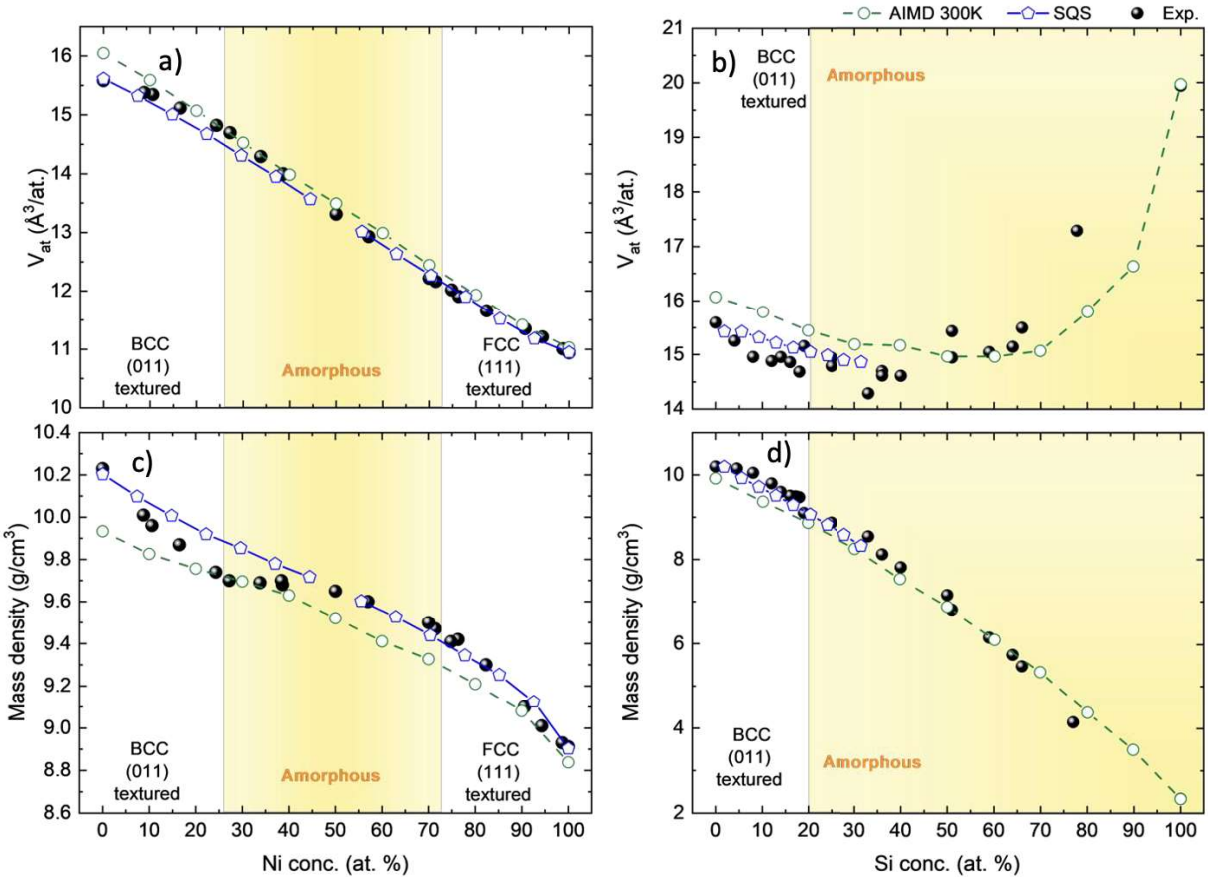

Figure 6: Comparison between experimental (black plain symbol) [4, 6, 10, 16] and first-principles calculations (dashed line for amorphous state designed by AIMD and full-line for crystalline state designed by SQS and DFT methods) of atomic volume (a-b) and mass density (c-d) for $Mo_{1-x}Ni_x$ and $Mo_{1-x}Si_x$ alloys.

This non-monotonous behavior cannot be predicted by a simple Vegard's rule of mixture and is partially attributed to the modifications of electronic properties governing the metallic (or covalent) character in Mo-Si alloys and to its structural state, crystalline or amorphous, both depending on Si content. Indeed, the observed minimum of experimental atomic volume for $x_{Si} \sim 0.3$-0.4 in the amorphous compositional range is much closer to the theoretical value of the denser crystalline phase than of the amorphous one. It may suggest the (co-)existence of a nanocrystalline phase nearby the phase transition that we cannot easily reveal by XRD. For $0.19 \leq x_{Si} \leq 0.7$, the metallic character of the amorphous alloys with a high Mo-centered clusters coordination number is maintained, and the atomic volume is only slightly affected by Si addition. For $x_{Si} > 0.7$, an increase in the atomic volume is progressively observed and the amorphous alloys acquire a covalent character and a reduced coordination number down to 4 (as shown in Figure 4). One can notice that for $x_{Si} \sim 0.80$ the experimental atomic volume is higher than the calculated one. It is not excluded that such a high value could be attributed to an excess of a-Si having higher volume with formation of depleted sub-silicides such as $MoSi_2$, Mo_3Si or Mo_5Si_3 [41].

3.4 Sound velocities and elastic constants

The measured [4, 6, 10, 16] and calculated longitudinal (V_L) and shear (V_S) sound velocities of Mo-Ni and Mo-Si alloys are shown in Figure 7 as black circles. The structural transitions from BCC to amorphous state observed for $x_{Si} \sim 0.19$ and $x_{Ni} \sim 0.27$, and from FCC to amorphous state observed for $x_{Ni} \sim 0.73$, are all accompanied by a reduction of sound velocities, when Ni or Si solute element is added to Mo or when Mo is added to Ni or Si. V_L is reduced from 6400 to 5700 m/s in Mo(Ni) and from 6700 to 5600 m/s in Ni(Mo), while V_S is reduced from 3100 to 2200 m/s in Mo(Ni) and from 2800 to 2100 m/s in Ni(Mo). In Mo(Si), V_L is reduced from 6300 to 5700 m/s, while V_S is reduced from 3300 to 2500 m/s. The trends

in the crystalline or the amorphous region are well captured by our calculations, whereas the spread between relaxed (lower value) and non-relaxed (upper value) calculated data is much wider for the amorphous structure than for the crystalline ones (BCC and FCC), due to non-equivalent atomic positions and related local relaxations, in the supercell of amorphous materials. One should notice that a quantitative agreement between experiments and calculations is achieved in the BCC-Mo(Si) ($0.19 \geq x_{Si} \geq 0$) with a <011>-texture, while it is not the case for the BCC-Mo(Ni) ($0.27 \geq x_{Ni} \geq 0$) with <011>-texture and FCC-Ni(Mo) ($1 \geq x_{Ni} \geq 0.75$) having <111>-texture.

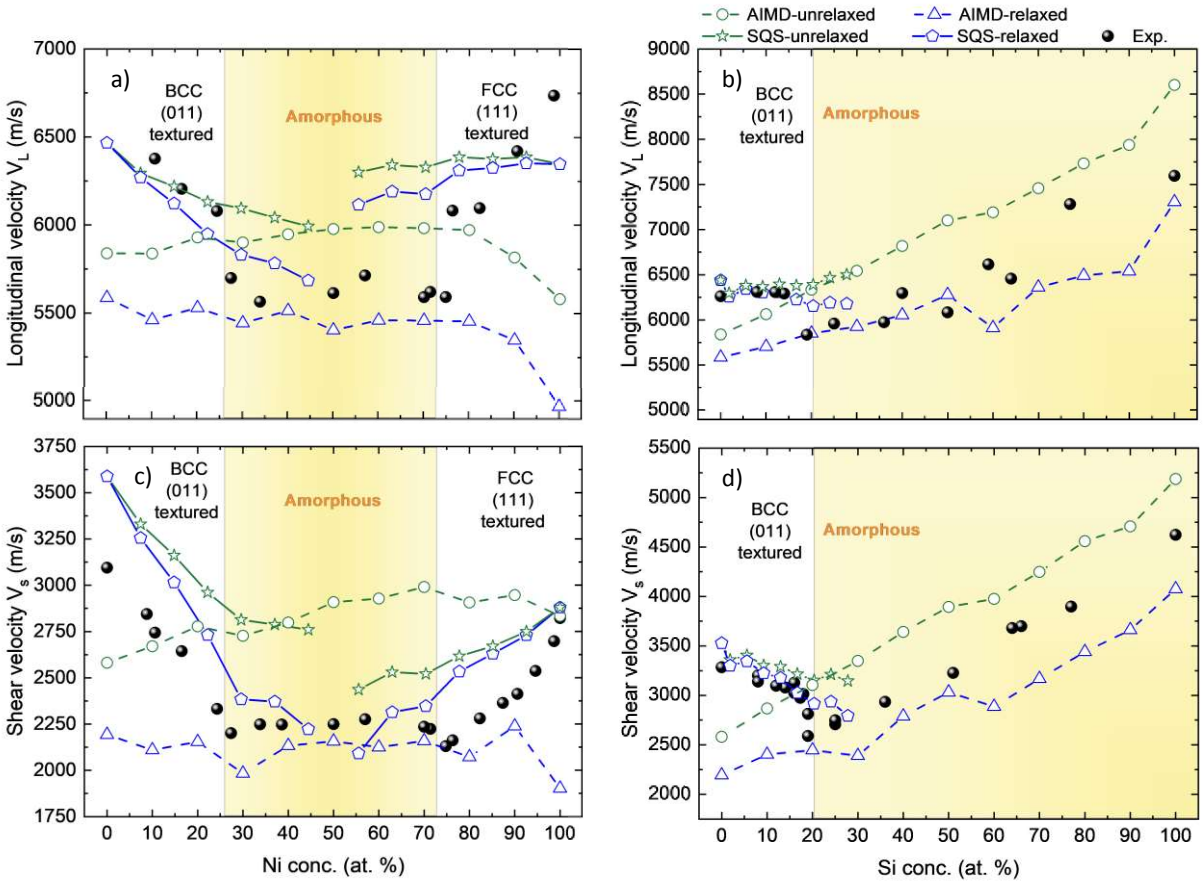

Figure 7: Comparison between experimental (black plain symbol) [4, 6, 10, 16] and first principles calculations (dashed line for amorphous state structure designed by AIMD and full-line for crystalline state designed by SQS and DFT methods) of longitudinal (a-b) and shear sound velocities (c-d) for $Mo_{1-x}Ni_x$ and $Mo_{1-x}Si_x$ alloys.

The observed differences can be ascribed to the presence of point defects (of interstitial types) introduced by energetic bombardment during growth of MoNi alloys by ion beam sputtering process, as was reported by Debelle *et al.* for pure Mo layers [42], and affecting more elastic properties of the crystalline phase than of the amorphous one. Intrinsic stress induced during film growth can also affect elastic properties [43]. Quantitative assessment of such complicate effects on sound velocities and elastic constants, as we performed in the case of defective-nitrides materials such as TaN [44] and MoAlN [45], is out the scope of this work.

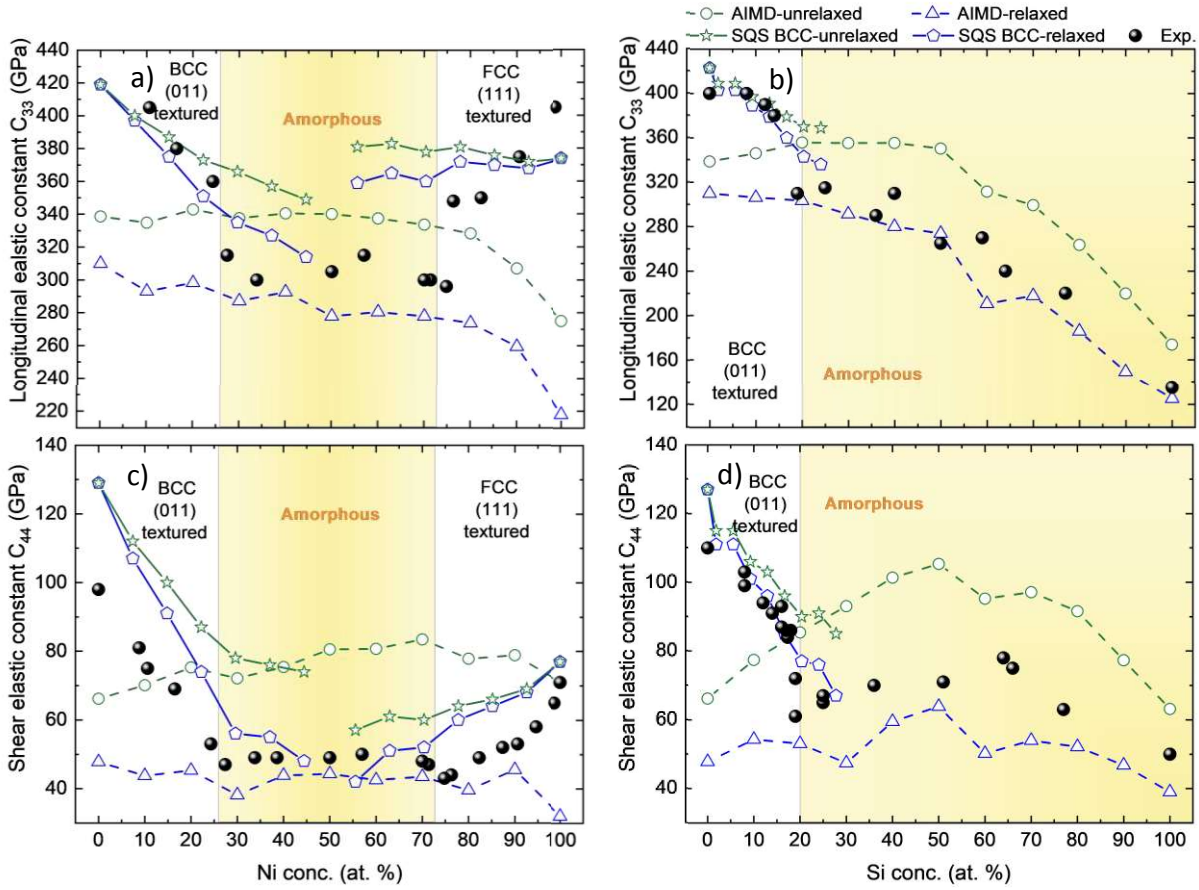

Figure 8: Comparison between experimental (black plain symbol) [4, 6, 10, 16] and first principles calculations (dashed line for amorphous state designed by AIMD and full-line for crystalline state designed by SQS and DFT methods) of longitudinal (a-b) and shear elastic constants (c-d) for $Mo_{1-x}Ni_x$ and $Mo_{1-x}Si_x$ alloys.

Similar softening trends of out-of-plane longitudinal modulus $C_{33} = \rho(V_L)^2$, and out-of-plane shear modulus $C_{44} = \rho(V_S)^2$ shown in Figure 8, are observed because of the simultaneous and monotonous decrease of the mass density. Again, the trends in the crystalline or the amorphous regions are well captured by our calculations, whereas the spread between relaxed and non-relaxed calculated data is much wider for the amorphous structures than for the crystalline ones. In the crystalline regions, a pronounced softening of C_{44} from 110 to 60 GPa for Mo-Si and from 65 to 45 GPa for Mo-Ni, is observed in the BCC region. C_{33} experiences a softening from 420 (ion beam sputtered-pure Mo) to 300 GPa for Mo-Si and from 400 (magnetron sputtered-pure Mo) to 280 GPa for Mo-Ni, respectively, while in FCC region, the C_{33} softens from 400 (pure Ni) to 300 GPa. For amorphous Mo-Ni alloys, elastic constants do not change much, while for Mo-Si, they exhibit two distinct behaviors depending on the electronic properties, metallic or covalent bonding character and atomic coordination number (see Figure 4). For $0.19 \leq x_{Si} \leq 0.7$, the metallic glass character of the alloys is maintained with a coordination number of polyhedral clusters in the range 12-15, as in the amorphous compositional range of Mo-Ni, and the elastic properties are remarkably stable. For $x_{Si} > 0.7$, while the Si-centered atomic volume first does not change (see Figure 3), an increase in the atomic volume is progressively observed and the amorphous alloys acquire a covalent character and a reduced coordination number down to 4. We are again witnessing a progressive softening of the elastic stiffness constants while, surprisingly, both the longitudinal and shear acoustic velocities increase continuously. All these behaviors are intrinsic consequences of the high Si, Ni and Mo supersaturation, leading to lattice instability and accompanying the phase transitions.

3.5 Metal to insulator transition in Mo-Si

In **supplementary materials "Electronic density of states"**, we report the calculated total (TDOS) and partial (PDOS) electronic density of states N(E) in the amorphous compositional

range of the Mo-Si system, as well as the previously measured electrical resistivity of Mo-Si alloys [16]. TDOS displays metallic and semi-metallic behavior as evidenced by the absence of a gap at the Fermi energy E_F. According to Mott *et al.* [46], static conductivity can be defined by the following expression:

$$\sigma_{dc} = \frac{4\pi^2\hbar^3 e^2}{3m^2} \mathrm{d}_{av} \left(\mathrm{N}(E_F)\right)^2$$

with $\hbar$ the reduced Planck constant, d_{av} the average interatomic distance, m the electron mass, e the electron charge, N(E_F) the density of states at Fermi energy. We calculated the electrical resistivity $\rho_e = 1/\sigma_{dc}$ shown in figure 9, that can satisfactory reproduce the trends of the measured electrical resistivity at 300K in the amorphous region [16]. In the range $0.20 < x_{Si} < 0.40$, the resistivity increases only slightly with the Si content x, pointing out the metallic character of these amorphous alloys. This behavior is commonly observed in highly resistive amorphous metallic alloys, in good agreement with the Mooij correlation [47], with an electron mean-free path of the order of the interatomic spacing. There is a transition for $0.9 > x_{Si} > 0.4$, as the electrical resistivity is increasing continuously, as well as atomic coordination is decreasing and atomic volume increasing. A sudden jump above x_{Si}~0.9 to a-Si is observed, when tetravalent atomic coordination (Figure 4) is reached with the highest atomic volume (Figure 6), showing that the metal to insulator transition is expected for x_{Si}~0.9.

4. Summary and conclusions

SQS and AIMD methods were used to design the supercells of crystalline and amorphous structures of Mo-Ni and Mo-Si alloys, together with DFT, to calculate their ground state properties (atomic volume, mass density, average interatomic distance, polyhedral cluster

analysis and electronic density of states), their sound velocities and elastic properties. We could elucidate the complex interrelationships between short-range atomic order properties and measured macroscopic properties in their amorphous states.

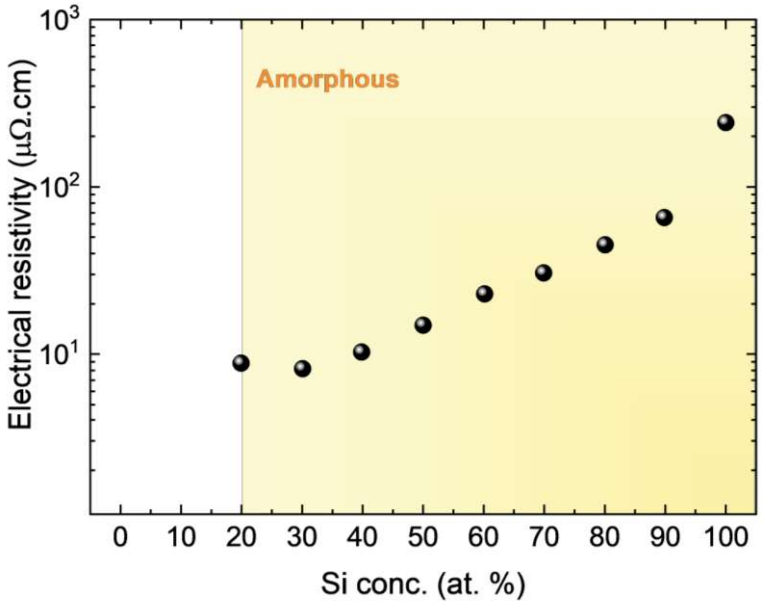

Figure 9: Calculated dc-electrical resistivity of Mo-Si amorphous alloys versus Si concentration.

The complex non-monotonic variation of atomic volume of Mo-Si, being non-predictable by a simple Vegard's rule of mixture, could be partially reproduced by our calculations, highlighting a plausible partial demixion in Si-rich alloys.

For both supersaturated polycrystalline alloys, calculated effective elastic constants, C_{33} and C_{44}, exhibit important softening upon incorporation of Ni or Si in Mo BCC lattice until phase transition to the amorphous state. It is supporting the huge softening observed in (Mo/Ni) multilayers, originating from the stabilization at the interface of metastable amorphous or polycrystalline Mo-Ni solid solutions, a few nm thick.

While a quantitative agreement is found for BCC Mo-Si alloys between our calculated elastic constants and the measured values [4, 6, 10, 16], it is not the case for BCC Mo(Ni) and FCC Ni(Mo). Any wrong or approximate assumption about crystallographic texture is not the cause of the discrepancy, leading to the consideration that the incorporation of point-defects are likely responsible for such deviation, in the case of Mo-Ni films obtained under highly energetic deposition process (ion-beam sputtering).

For both amorphous alloys, we calculated elastic constants in two ways, considering the possibility of atoms to relax (softer values) or not relax (stiffer values) after the application of elastic strains. The spread between upper and lower values is much larger in comparison to the polycrystalline case, but the trends are similar and account for the experimental data [4, 6, 10, 16]. C_{33} and C_{44} exhibit only a limited variation in the amorphous compositional range. Nevertheless, an additional softening is confirmed by our calculations for the Mo-Si system at the transition from metallic-to-covalent bonding character observed at x_{Si}~0.7, with a reduction of the atomic coordination from 12-15 for the polyhedral clusters in the metallic glass, to 4 for covalent a-Si.

For Mo-Si amorphous alloys, electronic density of states shows no gap at the Fermi level, confirming their metallic character. Their electrical resistivity is increasing with Si addition and the metal to insulator transition is found to occur for higher content of Si, $x_{Si} > 0.9$.

Overall, these numerical results provide an additional and comprehensive illustration of computational efficiency, relying on the combination of first-principles calculations (DFT and AIMD) and special quasi-random structures methods for designing amorphous structure and random alloys supercells, and the prediction of their structural and elastic properties

5. References

[1] I.K. Schuller, A. Fartash, M. Grimsditch, Elastic anomalies in superlattices, MRS Bulletin 15(10) (1990) 33-37.
[2] B. Perrin, B. Bonello, J.-C. Jeannet, E. Romatet, Picosecond ultrasonics study of metallic multilayers, Physica B: Condensed Matter 219 (1996) 681-683.
[3] B.M. Clemens, G.L. Eesley, Relationship between interfacial strain and the elastic response of multilayer metal films, Physical review letters 61(20) (1988) 2356.
[4] G. Abadias, C. Jaouen, F. Martin, J. Pacaud, P. Djemia, F. Ganot, Experimental evidence for the role of supersaturated interfacial alloys on the shear elastic softening of Ni/Mo superlattices, Physical Review B 65(21) (2002) 212105.
[5] F. Martin, C. Jaouen, J. Pacaud, G. Abadias, P. Djemia, F. Ganot, Strain, interdiffusion, and microstructural evolution under ion irradiation in Ni (111) / Mo (110) multilayers: Interdependence with elastic properties, Physical Review B 71(4) (2005) 045422.
[6] L. Belliard, A. Huynh, B. Perrin, A. Michel, G. Abadias, C. Jaouen, Elastic properties and phonon generation in Mo/Si superlattices, Physical Review B 80(15) (2009) 155424.
[7] C. Rossignol, B. Perrin, B. Bonello, P. Djemia, P. Moch, H. Hurdequint, Elastic properties of ultrathin permalloy/alumina multilayer films using picosecond ultrasonics and Brillouin light scattering, Physical Review B 70(9) (2004) 094102.
[8] J. Slaughter, D.W. Schulze, C. Hills, A. Mirone, R. Stalio, R. Watts, C. Tarrio, T.B. Lucatorto, M. Krumrey, P. Mueller, Structure and performance of Si/Mo multilayer mirrors for the extreme ultraviolet, Journal of applied Physics 76(4) (1994) 2144-2156.
[9] B.r. Krause, G. Abadias, A. Michel, P. Wochner, S. Ibrahimkutty, T. Baumbach, Direct observation of the thickness-induced crystallization and stress build-up during sputter-deposition of nanoscale silicide films, ACS Applied Materials & Interfaces 8(50) (2016) 34888-34895.
[10] S. Laborde, Acoustique picoseconde dans les multicouches métalliques, Université Pierre et Marie Curie-Paris VI, 2006.
[11] B. Zhao, F. Zeng, F. Pan, Formation of metastable alloy films in the Ni-Mo binary system by ion-beam-assisted deposition, Applied Physics A 77 (2003) 523-528.
[12] Q. Zhang, Z. Li, C. Lin, B. Liu, E. Ma, Glass-forming range of the Ni–Mo system derived from molecular dynamics simulation and generalized lindemann criterion, Journal of Applied Physics 87(9) (2000) 4147-4152.
[13] W. Zhao, W. Li, Z. Sun, S. Gong, L. Vitos, Tuning the plasticity of Ni-Mo solid solution in Ni-based superalloys by ab initio calculations, Materials & design 124 (2017) 100-107.
[14] W. Zhao, W. Li, X. Li, S. Gong, L. Vitos, Z. Sun, Thermo-mechanical properties of Ni-Mo solid solutions: A first-principles study, Computational materials science 158 (2019) 140-148.
[15] K. Yaqoob, J.-C. Crivello, J.-M. Joubert, Thermodynamic modeling of the Mo–Ni system, Calphad 62 (2018) 215-222.
[16] A. Fillon, C. Jaouen, A. Michel, G. Abadias, C. Tromas, L. Belliard, B. Perrin, P. Djemia, Lattice instability and elastic response of metastable Mo 1− x Si x thin films, Physical Review B 88(17) (2013) 174104.
[17] H. Okamoto, Mo-Si (Molybdenum-Silicon), Journal of Phase Equilibria and Diffusion 32 (2011) 176-176.
[18] G. Kresse, J. Furthmüller, Efficient iterative schemes for ab initio total-energy calculations using a plane-wave basis set, Physical Review B 54(16) (1996) 11169.
[19] A. Van de Walle, P. Tiwary, M. De Jong, D. Olmsted, M. Asta, A. Dick, D. Shin, Y. Wang, L.-Q. Chen, Z.-K. Liu, Efficient stochastic generation of special quasirandom structures, Calphad 42 (2013) 13-18.
[20] J.P. Perdew, K. Burke, M. Ernzerhof, Generalized gradient approximation made simple, Physical review letters 77(18) (1996) 3865.

[21] Y. Le Page, P. Saxe, Symmetry-general least-squares extraction of elastic data for strained materials fromab initiocalculations of stress, Physical Review B 65(10) (2002).
[22] R. Hill, The elastic behaviour of a crystalline aggregate, Proceedings of the Physical Society. Section A 65(5) (1952) 349.
[23] J.D. Schall, G. Gao, J.A. Harrison, Elastic constants of silicon materials calculated as a function of temperature using a parametrization of the second-generation reactive empirical bond-order potential, Physical Review B 77(11) (2008) 115209.
[24] G. De Sandre, L. Colombo, C. Bottani, Calculation of elastic constants in defected and amorphous silicon by quantum simulations, Physical Review B 54(17) (1996) 11857.
[25] J. Houska, S. Kos, Ab initio modeling of complex amorphous transition-metal-based ceramics, Journal of Physics: Condensed Matter 23(2) (2010) 025502.
[26] A. Stukowski, Visualization and analysis of atomistic simulation data with OVITO–the Open Visualization Tool, Modelling and Simulation in Materials Science and Engineering 18(1) (2010) 015012.
[27] G. Guo, Quasi-Icosahedral Clusters in Zr-Based Metallic Glasses, Metals 10(9) (2020) 1135.
[28] J.M. Lopez, J.A. Alonso, L.J. Gallego, Determination of the glass-forming concentration range in binary alloys from a semiempirical theory: Application to Zr-based alloys, Phys Rev B Condens Matter 36(7) (1987) 3716-3722.
[29] G. Van der Kolk, A. Miedema, A. Niessen, On the composition range of amorphous binary transition metal alloys, Journal of the Less Common Metals 145 (1988) 1-17.
[30] S. Kugler, L. Pusztai, L. Rosta, P. Chieux, R. Bellissent, Structure of evaporated pure amorphous silicon: Neutron-diffraction and reverse Monte Carlo investigations, Physical Review B 48(10) (1993) 7685.
[31] E.-a. Zen, Validity of "vegard's law", Mineralogical Society of America, 1956.
[32] Z.D. Sha, Y.P. Feng, Y. Li, Statistical composition-structure-property correlation and glass-forming ability based on the full icosahedra in Cu–Zr metallic glasses, Applied Physics Letters 96(6) (2010).
[33] T.-Y. Chang, Z. Wang, D. Xu, Icosahedral clusters in Cu100-xZrx (x=32,34,36,38.2,40 at.%) metallic glasses near the peak of glass-forming ability (x=36): A balance between population and encaging strength, Journal of Physics and Chemistry of Solids 154 (2021).
[34] H.L. Peng, M.Z. Li, W.H. Wang, C.Z. Wang, K.M. Ho, Effect of local structures and atomic packing on glass forming ability in CuxZr100−x metallic glasses, Applied Physics Letters 96(2) (2010).
[35] J. Houska, P. Machanova, M. Zitek, P. Zeman, Molecular dynamics and experimental study of the growth, structure and properties of Zr–Cu films, Journal of Alloys and Compounds 828 (2020) 154433.
[36] M.H. Abbasi, S.G. Shabestari, R. Tavakoli, On the glass-forming ability of (Zr0.5Cu0.5)100−xAlx ternary alloys: A molecular dynamics study, Materials Today Communications 31 (2022).
[37] B. Arman, S.-N. Luo, T.C. Germann, T. Çağın, Dynamic response ofCu46Zr54metallic glass to high-strain-rate shock loading: Plasticity, spall, and atomic-level structures, Physical Review B 81(14) (2010).
[38] K.-W. Park, Effect of the Atomic Packing Density on the Structural Change Rate of Amorphous Alloys under Elastostatic Stress, Metals and Materials International 14(2) (2008) 159-163.
[39] K.-W. Park, J.-i. Jang, M. Wakeda, Y. Shibutani, J.-C. Lee, Atomic packing density and its influence on the properties of Cu–Zr amorphous alloys, Scripta Materialia 57(9) (2007) 805-808.

[40] G. Guo, Quasi-Icosahedral Clusters in Zr-Based Metallic Glasses, Metals 10(9) (2020).
[41] S. Govindarajan, B. Mishra, D. Olson, J. Moore, J. Disam, Synthesis of molybdenum disilicide on molybdenum substrates, Surface and Coatings Technology 76 (1995) 7-13.
[42] A. Debelle, G. Abadias, A. Michel, C. Jaouen, Stress field in sputtered thin films: Ion irradiation as a tool to induce relaxation and investigate the origin of growth stress, Applied physics letters 84(24) (2004) 5034-5036.
[43] G. Abadias, E. Chason, J. Keckes, M. Sebastiani, G.B. Thompson, E. Barthel, G.L. Doll, C.E. Murray, C.H. Stoessel, L. Martinu, Stress in thin films and coatings: Current status, challenges, and prospects, Journal of Vacuum Science & Technology A 36(2) (2018).
[44] G. Abadias, C.-H. Li, L. Belliard, Q.M. Hu, N. Grenèche, P. Djemia, Large influence of vacancies on the elastic constants of cubic epitaxial tantalum nitride layers grown by reactive magnetron sputtering, Acta Materialia 184 (2020) 254-266.
[45] F. Anğay, L. Löfler, F. Tetard, D. Eyidi, P. Djemia, D. Holec, G. Abadias, Structure, stress, and mechanical properties of Mo-Al-N thin films deposited by dc reactive magnetron cosputtering: Role of point defects, Journal of Vacuum Science & Technology A 38(5) (2020).
[46] N.F. Mott, E.A. Davis, Electronic processes in non-crystalline materials, Oxford university press2012.
[47] P. Cote, L. Meisel, Glassy Metals I ed HJ Guntherodt and H Beck, Heidelberg: Springer 46 (1981) 141-66.